

Quasi-one-dimensional electronic structure of hollandite ruthenate $K_2Ru_8O_{16}$ T. Toriyama,¹ M. Watanabe,¹ T. Konishi,² and Y. Ohta¹¹*Department of Physics, Chiba University, Chiba 263-8522, Japan*²*Graduate School of Advanced Integration Science, Chiba University, Chiba 263-8522, Japan*

(Received 16 March 2011; revised manuscript received 30 March 2011; published 2 May 2011)

The electronic structure of hollandite ruthenate $K_2Ru_8O_{16}$ is calculated using the generalized gradient approximation (GGA) in the density functional theory, where the Hubbard-type repulsive interaction is taken into account (GGA+ U). We find that the electronic structure near the Fermi level consists only of a single band coming predominantly from the $4d_{yz}$ and $4d_{zx}$ orbitals of Ru ions with a strong admixture of the $2p_z$ orbitals of corner-shared O ions connecting the double RuO chains. The band structure near the Fermi level is highly quasi-one-dimensional, exactly at half filling, and has a pair of two nearly parallel sheetlike Fermi surfaces separated by π/c . The calculated results are consistent with observed quasi-one-dimensional transport properties of the material. These results establish that $K_2Ru_8O_{16}$ belongs to a class of possible Tomonaga-Luttinger-liquid materials.

DOI: [10.1103/PhysRevB.83.195101](https://doi.org/10.1103/PhysRevB.83.195101)

PACS number(s): 71.20.-b, 71.27.+a, 71.10.Pm, 71.20.Be

I. INTRODUCTION

The electronic states of transition-metal oxides with a hollandite-type crystal structure have attracted considerable attention in recent years. The crystal structure of hollandites (see Fig. 1) resembles that of the rutile structure but the single chains of MO_6 octahedra (M = transition element) in rutiles are replaced by the double chains of the edge-shared MO_6 octahedra in hollandites, resulting in a sparse structure with large tunnels, wherein a variety of cations A can be introduced as in the chemical formula $A_xM_8O_{16}$ with $0 \leq x \leq 2$. The materials are thus known to be useful for potential applications, e.g., for making batteries.

The hollandite materials have also attracted attention in the field of physics of strong electron correlations because the material series with the $3d$ transition-metal elements M = Ti, V, Cr, and Mn, which are in a mixed valent state, show a variety of unusual electronic and magnetic properties: In the Ti series, $K_xTi_8O_{16}$ has been reported to be either a dilute ferromagnetic semiconductor¹ or a paramagnetic metal,² depending on the carrier concentration. In the V series, $K_2V_8O_{16}$ shows a variety of physical properties associated with the metal-insulator transition.²⁻¹⁰ In the Cr series, $K_2Cr_8O_{16}$ has been reported to exhibit phase transitions from metallic paramagnet to ferromagnet and then to insulating ferromagnet by lowering temperatures.^{11,12} In the Mn series, a variety of structural, electronic, and magnetic phase transitions have been reported as well.^{13,14}

The material series with the $4d$ transition-metal elements M = Mo, Ru, and Rh also show interesting physical properties: In the Mo series, a Mo_4 clustering has been reported to occur in $Rb_{1.5}Mo_8O_{16}$.¹⁵ In the Ru series, a quasi-one-dimensional electron conduction has been reported in KRu_4O_8 , $RbRu_4O_8$, and $Cs_{0.8}Li_{0.2}Ru_4O_8$,^{16,17} as well as in $BaRu_6O_{12}$ (Ref. 18) with a similar crystal structure. In the Rh series, a quasi-one-dimensional electron conduction has also been reported.¹⁹⁻²²

However, although the experimental data have thus been accumulated, to the best of our knowledge, no theoretical calculations on the electronic structure of these materials, in particular for the $4d$ transition-metal oxides, have been made

so far, and little is known about their electronic states for understanding the anomalous electronic properties observed experimentally.

In this paper, we therefore make the electronic structure calculations on these materials, focusing in particular on a ruthenate material $K_2Ru_8O_{16}$. This material has a body-centered tetragonal crystal structure and all the Ru sites are crystallographically equivalent (see Fig. 1).^{16,17,23} The Ru ions are in the mixed valent state with an average valence of $Ru^{3.75+}$ ($d^{4.25}$), i.e., there are formally Ru^{4+} (d^4) and Ru^{3+} (d^5) in a 3 : 1 ratio. Quasi-one-dimensional electronic properties have been reported recently:¹⁶ The temperature dependence of the electric resistivity along the chain direction always decreases with decreasing temperature, whereas that perpendicular to the chains increases with decreasing temperature down to ~ 180 K, indicating the quasi-one-dimensionality of the electron conduction of the system. The anisotropy ratio of the resistivity has been reported to be ~ 34 (~ 20) at 4.2 K (150 K).

To clarify the origins of the properties of this material, we make the electronic structure calculations employing the WIEN2K code,²⁴ where we use the generalized gradient approximation (GGA) in the density functional theory, taking into account the Hubbard-type repulsive interaction (GGA+ U).²⁵ We will thereby show that, despite its structural complexity, the electronic state of $K_2Ru_8O_{16}$ near the Fermi level is surprisingly simple, consisting only of a single band coming predominantly from the $4d_{yz}$ and $4d_{zx}$ orbitals of Ru ions with a strong admixture of the $2p_z$ orbitals of corner-shared O ions connecting the double RuO chains. The electronic band structure near the Fermi level is highly quasi-one-dimensional, exactly at half filling, and has a pair of nearly parallel sheetlike Fermi surfaces separated by π/c . The calculated results are consistent with observed quasi-one-dimensional electron conduction of this material. These results establish that $K_2Ru_8O_{16}$ belongs to a class of materials for further studies of Tomonaga-Luttinger liquids.²⁶ We also calculate the optical conductivity spectrum, which we hope will encourage further experimental studies of this interesting material.

This paper is organized as follows: We present some details of our method of calculations in Sec. II and present the

results of calculations for the electronic structures in Sec. III. Discussion on the relations to the other materials is given in Sec. IV, and summary of the paper is given in Sec. V.

II. METHOD OF CALCULATION

We employ the computer code WIEN2K²⁴ based on the full-potential linearized augmented-plane-wave (FLAPW) method. We have tested both the local density approximation (LDA) and generalized gradient approximation (GGA) for the exchange-correlation potential²⁷ in the density functional theory. In this paper, we will present only the results of GGA because no significant differences are found between the two. We use the experimental crystal structure of $\text{K}_2\text{Ru}_8\text{O}_{16}$ observed at room temperature with lattice constants $a = 9.866$ and $c = 3.131$ Å.²³ The symmetry of the lattice is body centered tetragonal ($I4/m$ space group, see Fig. 1). The primitive unit cell contains four Ru ions, one K ion, and eight O ions. All the Ru ions are crystallographically equivalent, but there are two inequivalent O ions, i.e., O(1) inside the double chains and O(2) connecting the double chains. In the self-consistent calculations, we use 1,060 k points in the irreducible part of the Brillouin zone (see Fig. 1) with an anisotropic sampling to achieve better convergence. We use the plane-wave cutoff of $K_{\max} = 3.65$ Bohr⁻¹. To improve the description for the electron correlations in the Ru $4d$ orbitals, we use the rotationally invariant version of the GGA+ U method with the double-counting correction in the fully localized limit,^{25,28} assuming a value $U = 3.0$ eV for the Ru $4d$ orbitals. We use the codes VESTA²⁹ and XCRYSDEN³⁰ for graphical purposes.

III. RESULTS OF CALCULATION

A. Density of states

The calculated results for the densities of states (DOS) are shown in Fig. 2(a) in a wide energy (ε) range. We find that the Ru $4d$ band is located at $-2 \lesssim \varepsilon \lesssim 5$ eV and is well separated from the O $2p$ band located at $-8 \lesssim \varepsilon \lesssim -2.5$ eV, with considerable hybridization between Ru $4d$ and O $2p$ orbitals. We also find that the t_{2g} bands of Ru $4d$ electrons are well separated from the e_g bands, corresponding to a large value of the crystal-field splitting of $10D_q \simeq 3$ eV. Thus, the low-energy properties of this system are essentially governed by the three t_{2g} orbitals, d_{xy} , d_{yz} , and d_{zx} of Ru ions, hybridized strongly with the O $2p$ orbitals, where we use the coordinate system (x, y, z) defined in Ref. 12.

The calculated orbital-decomposed partial densities of states (PDOS) near the Fermi level are shown in Figs. 2(b)–2(d). We first find that the total t_{2g} PDOS curve has a deep valley of a width of ~ 0.4 eV around the Fermi level, and thus the DOS at the Fermi level is rather low, 6.48 states/eV/f.u. at $U = 0$ eV and 4.52 states/eV/f.u. at $U = 3$ eV. We also find that the d_{xy} component locates substantially below the Fermi level, whereas the d_{yz} and d_{zx} components, which are exactly degenerate,⁹ extend over the t_{2g} bands. The d_{xy} component at $U = 0$ eV has a peak at ~ -0.4 eV, which becomes broader and shifts to lower energies at $U = 3$ eV, indicating that the d_{xy} orbital is almost fully occupied by electrons when U is sufficiently large.

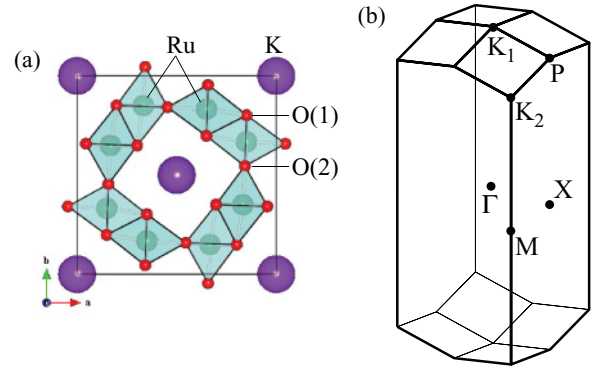


FIG. 1. (Color online) Schematic representation of (a) the crystal structure and (b) Brillouin zone of $\text{K}_2\text{Ru}_8\text{O}_{16}$. In (b), the symbols represent $\Gamma(0, 0, 0)$, $M(2\pi/a, 0, 0)$, $X(\pi/a, \pi/a, 0)$, $P(\pi/a, \pi/a, \pi/c)$, $K_1[0, 0, \pi(1/c + c/a^2)]$, and $K_2[2\pi/a, 0, \pi(1/c - c/a^2)]$, where K_1 and K_2 are equivalent.

The calculated PDOS for O(1) (inside the double chains) and O(2) (bridging the double chains) are shown in Figs. 2(c) and 2(d), respectively. The p_x and p_y components are exactly degenerate for both O(1) and O(2). We find that for O(1) the components of p_x , p_y , and p_z are more or less extended over the whole t_{2g} region but for O(2) the p_z component resides predominantly above the Fermi level, whereas the p_x and p_y components have very small weight above the Fermi level, indicating that a large number of holes reside in the p_z orbital of O(2). This result suggests that the p_z orbital of O(2) is in a negative charge-transfer gap situation,³¹ as in the case of $\text{K}_2\text{Cr}_8\text{O}_{16}$.¹² In the latter, the valence electrons are fully spin polarized and therefore the Fermi level is located between the third and fourth bands counted from the top of the 12 t_{2g} bands for majority-spin electrons.¹²

B. Band dispersion

The calculated band dispersion near the Fermi energy is shown in Fig. 3. We find that there are 12 bands coming mainly from the Ru $4d$ t_{2g} orbitals (which we call the t_{2g} manifold) and the Fermi level crosses only the fourth band counted from the top and thus the fourth band is exactly at half filling. The fourth band is highly dispersive along the Γ - K_1 , X - P , and M - K_2 lines and weakly dispersive along the Γ - X , P - K_1 , and K_1 - K_2 lines, reflecting the quasi-one-dimensionality of the electronic state of this material. This result is consistent with the observed large anisotropy of the electric resistivity of the single crystal of this material.¹⁶

To describe the band structure more precisely, we note that the uppermost four bands in the t_{2g} manifold come predominantly from the d_{yz} and d_{zx} orbitals of Ru hybridized strongly with the p_z orbital of O(2) and that the first and fourth bands counted from the top are highly dispersive and the second and third bands are less dispersive. This characteristic band structure can roughly be understood by the tight-binding model consisting of the d_{yz} , d_{zx} , and p_z orbitals of an isolated column made of four Ru-O(2) chains running along the axis, of which the column structure can be realized if each of the Ru-O double chains in hollandite is cut into two at O(1) and the resulting four single Ru-O(2) chains are gathered to form the column structure of the four Ru-O(2) chains, as in the rutile

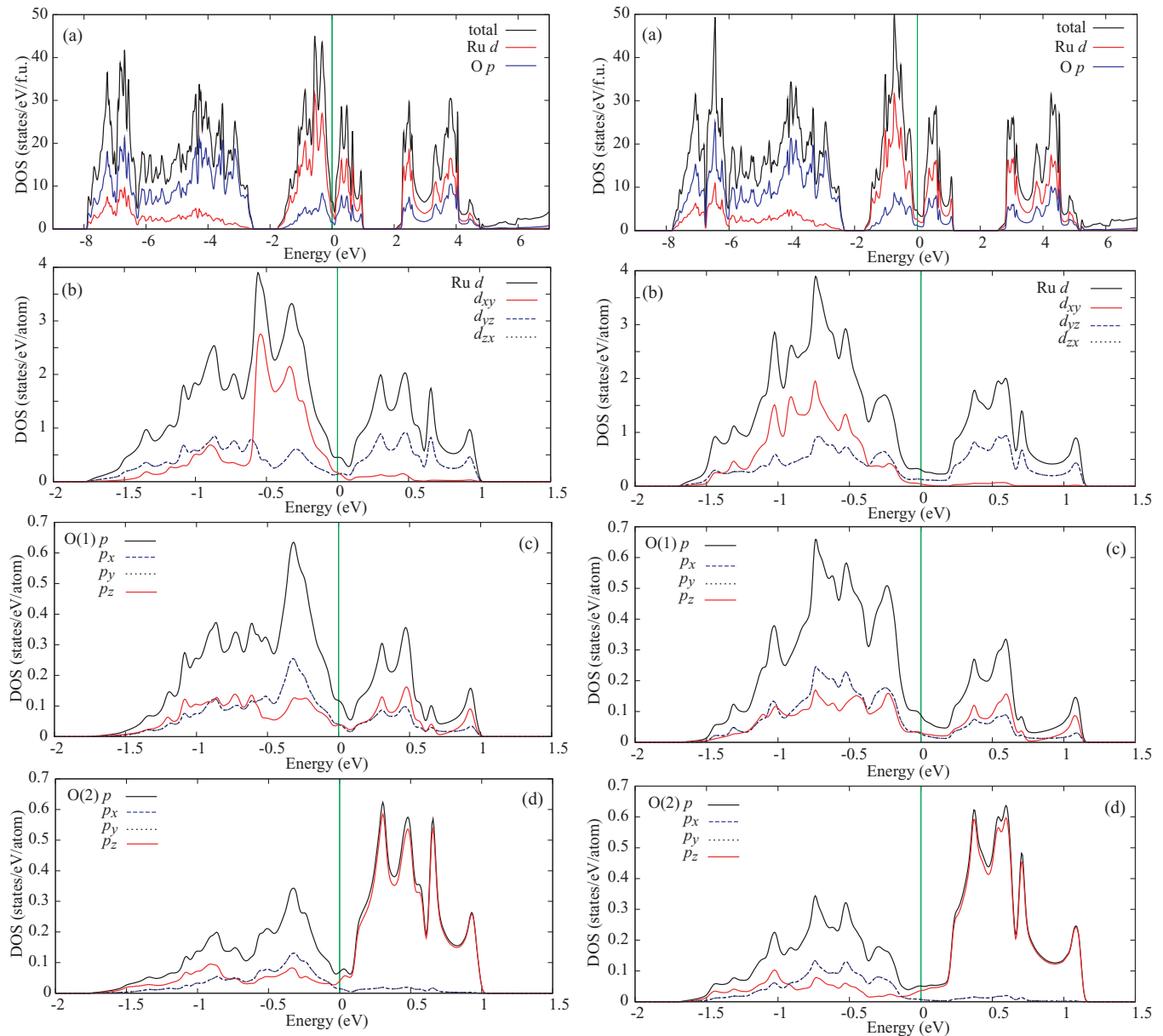


FIG. 2. (Color online) Calculated DOS and PDOS at $U = 0$ eV (left-hand panel) and at $U = 3$ eV (right-hand panel). (a) DOS [per formula unit (f.u.)] of $\text{K}_2\text{Ru}_8\text{O}_{16}$ in a wide energy range. (b) PDOS for Ru d t_{2g} orbitals near the Fermi level, where contributions from the d_{yz} and d_{zx} orbitals (thin dotted lines) are exactly degenerate. (c) PDOS for O(1), where contributions from the p_x and p_y orbitals are exactly degenerate. (d) PDOS for bridging oxygens O(2), where contributions from the p_x and p_y orbitals are exactly degenerate. The Fermi level is indicated by the vertical line.

structure. Thus, the coupling (or electron hopping) via the $2p$ orbitals of O(1) is rather small in $\text{K}_2\text{Ru}_8\text{O}_{16}$.

We also find in Fig. 3 that the fifth to eighth bands counted from the top of the t_{2g} manifold, which have a strong d_{xy} character, shift significantly to lower energies by increasing the value of U . Note that the fourth band then tends to be isolated in the energy bands and thus the one dimensionality is enhanced by increasing the value of U .

C. Fermi surface

The calculated results for the Fermi surface are shown in Fig. 4. We find that only the fourth band counted from the top of the t_{2g} manifold crosses the Fermi level to form the

Fermi surfaces. If the system were strictly one dimensional, a pair of the parallel Fermi surfaces should appear at $k_z = \pm k_F$ with $2k_F = \pi/c$. We actually find such a situation of the pair of the Fermi surfaces in Fig. 4, but the surfaces are considerably warped, indicating that the one dimensionality is not perfect, which we call the quasi-one-dimensional Fermi surfaces. We find that the one dimensionality is enhanced when the value of U increases. This system in the presence of electron correlations is therefore a good candidate for further studies of Tomonaga-Luttinger liquids.²⁶ We should point out that the nesting feature in the two nearly parallel Fermi surfaces seen in Fig. 4 does not lead to any instabilities in the actual material because the nesting is not perfect; if the nesting were

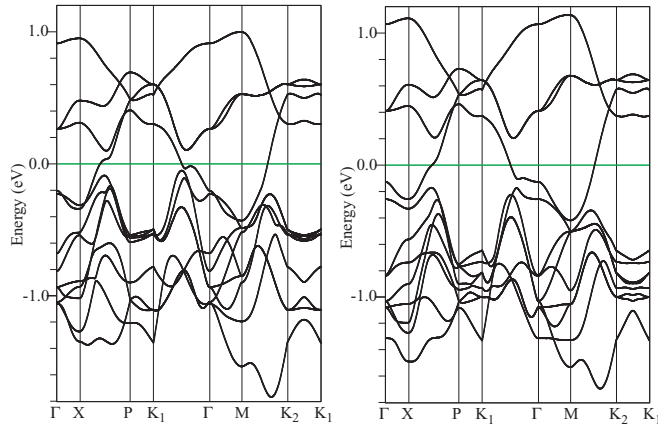


FIG. 3. (Color online) Calculated band dispersion of $\text{K}_2\text{Ru}_8\text{O}_{16}$ near the Fermi level (horizontal line) where the labels of the k points are shown in Fig. 1. The results at $U = 0$ eV (left-hand panel) and $U = 3$ eV (right-hand panel) are shown. There are 12 bands of the Ru $4d$ t_{2g} orbitals, where the fourth band from the top is at half filling.

sufficiently strong, the $2k_F$ instability would result in, e.g., the opening of the band gap, as in $\text{K}_2\text{Cr}_8\text{O}_{16}$.^{11,12}

D. Optical conductivity

We calculate the real part of the optical conductivity tensor $\text{Re } \sigma_{\alpha\beta}(\omega)$ in the random-phase approximation using the results of our electronic structure calculations.³² The results for the polarization parallel to the chains, $\sigma_{\parallel}(\omega)$, and perpendicular to the chains, $\sigma_{\perp}(\omega)$, are shown in Fig. 5, where both the interband and intraband (or Drude) contributions are included. For the Drude contributions, we assume the form

$$\text{Re } \sigma_{\alpha\beta}(\omega) = \frac{\omega_{p,\alpha\beta}^2}{4\pi} \frac{\Gamma}{\omega^2 + \Gamma^2}, \quad (1)$$

where $\omega_{p,\alpha\beta}$ is the plasma frequency calculated from the band structure and Γ is a lifetime broadening ($\Gamma = 0.05$ eV is assumed). The calculated values of the plasma frequency are 1.41 eV (1.08 eV) for the electric field along the c axis and 0.39 eV (0.16 eV) for the electric field perpendicular to the c axis at $U = 0$ eV ($U = 3$ eV).

We first find in Fig. 5 that the Drude contribution ($\omega \simeq 0$ eV) is strongly anisotropic, reflecting the anisotropic quasi-one-

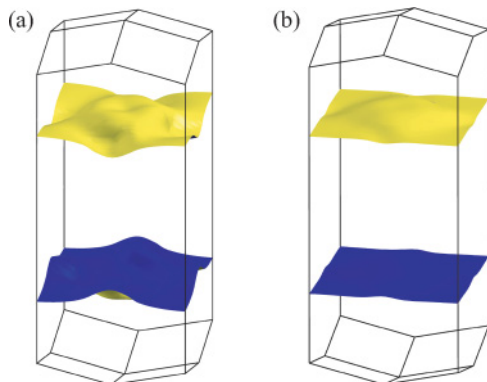


FIG. 4. (Color online) Calculated Fermi surfaces of $\text{K}_2\text{Ru}_8\text{O}_{16}$ at (a) $U = 0$ eV and (b) $U = 3$ eV.

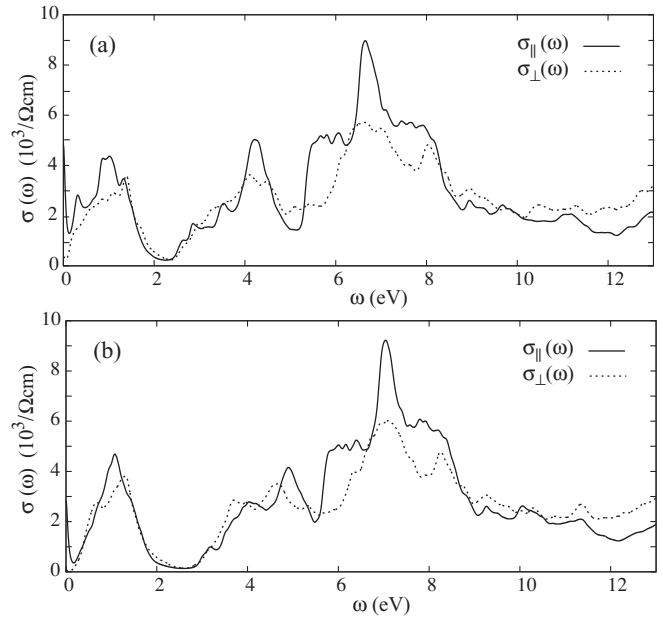


FIG. 5. Calculated optical conductivity $\sigma_{\parallel}(\omega)$ (electric field parallel to the c axis) and $\sigma_{\perp}(\omega)$ (electric field perpendicular to the c axis) of $\text{K}_2\text{Ru}_8\text{O}_{16}$ at (a) $U = 0$ eV and (b) $U = 3$ eV. Both the interband and intraband (or Drude) contributions are included.

dimensional band structure in the vicinity of the Fermi surface: The weight for the electric field parallel to the c axis is small but finite, whereas that perpendicular to the c axis is vanishingly small, in agreement with the observed anisotropic electron conduction.¹⁶ We then find that the spectra in the energy range of $0 < \omega \lesssim 2$ eV, apart from the Drude weight, come from the interband transitions among the 12 t_{2g} bands. The polarization dependence of the spectra is significant but not very strong. However, the U dependence of the spectra is very large: The weight at $\omega \lesssim 1$ eV is strongly suppressed with increasing U . This behavior may be understood because the peaklike structure for the d_{xy} component in the PDOS curve [see Fig. 2(b)] at $U = 0$ eV shifts to lower energies and becomes broadened by increasing the value of U . Such changes in the optical conductivity spectra may be noticed in other interband transitions, e.g., in the shift of the shoulderlike structure at $\omega \simeq 4$ eV. If the experimental optical conductivity spectrum is measured in this material, comparison with our theoretical results will therefore enable us to discuss the possible inadequacy of the approximations used and also to determine an appropriate value of U for this material. The spectra at $\omega \gtrsim 5$ eV do not have significant U dependence, but have some characteristic structures, as seen in Fig. 5. We hope that our calculated results will be compared with experiments made in the near future.

IV. DISCUSSION

Here we discuss some common features in the electronic structure of other hollandite materials, in particular, Rh oxides and Cr oxides, because in these materials the Fermi level is located somewhere in the uppermost four bands in the t_{2g} manifold that are of highly one-dimensional character

(see Sec. III B), and actually the quasi-one-dimensional electronic transport properties have been reported experimentally.

First, we discuss the hollandite rhodates. There are experimental reports on $\text{Ba}_{1.2}\text{Rh}_8\text{O}_{16}$,^{19,20} $(\text{Ba,Bi})_{1.54}\text{Rh}_8\text{O}_{16}$,²¹ and $\text{Sr}_{1.5}\text{Rh}_8\text{O}_{16}$.²² The formal oxidation state of Rh in these materials ranges between $\text{Rh}^{3.57+}$ ($d^{5.43}$) and $\text{Rh}^{3.7+}$ ($d^{5.3}$). The number of d electrons thus indicates that the second band counted from the top in the t_{2g} manifold crosses the Fermi level with the filling of electrons roughly between a half to three quarters if the second band is isolated (although of course more than one band can cross the Fermi level). Our preliminary electronic structure calculations indicate that the band structure is not very simple, but there are in fact highly quasi-one-dimensional bands, as expected from our results for $\text{K}_2\text{Ru}_8\text{O}_{16}$, which is consistent with the quasi-one-dimensional transport properties reported in $\text{Ba}_{1.2}\text{Rh}_8\text{O}_{16}$.^{19,20}

Another interesting example is the ferromagnetic hollandite $\text{K}_2\text{Cr}_8\text{O}_{16}$,¹¹ where Cr ions are in the oxidation state $\text{Cr}^{3.75+}$ ($d^{2.25}$). The electronic structure calculations¹² have shown that the system is a fully spin-polarized half metal and that the Fermi level is located between the third and fourth bands counted from the top of the t_{2g} manifold for majority-spin electrons, or that both of the third and fourth bands cross the Fermi level to form a semimetallic (or compensated metallic) band structure. In fact, it has been found¹² that the Fermi surface of the fourth band is highly quasi-one-dimensional, as in the present $\text{K}_2\text{Ru}_8\text{O}_{16}$.

We should note that such situations are in strong contrast to the hollandite vanadate $\text{K}_2\text{V}_8\text{O}_{16}$, where the Fermi level is located in the third band counted from the lowest in the t_{2g} manifold. It has been shown¹⁰ that the lowest four bands are predominantly of d_{xy} character and that the nesting of the Fermi surfaces may not play an important role in the observed metal-insulator transition. Effects of electron correlations would rather be more important in $\text{K}_2\text{V}_8\text{O}_{16}$.

Thus, the number of valence electrons or the location of the Fermi level, i.e., whether it is in the uppermost four bands or among the lowest four bands, determines the basic electronic properties of hollandite-type transition-metal oxides.

V. SUMMARY

We have calculated the electronic structure of hollandite ruthenate $\text{K}_2\text{Ru}_8\text{O}_{16}$ using GGA in the density functional

theory, taking into account the Hubbard-type repulsive interaction U . We have shown that, despite its structural complexity, the electronic structure of this material near the Fermi level is surprisingly simple, as summarized in the following: (i) The low-energy electronic states are essentially governed by the three t_{2g} orbitals d_{xy} , d_{yz} , and d_{zx} of Ru ions, which are separated largely from the e_g orbitals of Ru ions, but are strongly hybridized with the O $2p$ orbitals. (ii) The band structure near the Fermi level consists only of a single band coming predominantly from the $4d_{yz}$ and $4d_{zx}$ orbitals of Ru ions, with a strong admixture of the $2p_z$ orbitals of O(2) ions, and is highly quasi-one-dimensional and exactly at half filling. (iii) The Fermi surface is highly quasi-one-dimensional, consisting of a pair of two nearly parallel sheetlike surfaces separated by $2k_F = \pi/c$, consistent with the observed large anisotropy of the electric resistivity. The results thus establish that this system is in a class of Tomonaga-Luttinger liquids. (iv) The calculated optical conductivity spectrum shows a rather simple structure in the low-frequency region $\omega \lesssim 2$ eV with a highly anisotropic Drude weight. The characteristic structures are seen also in the high-frequency region. (v) The band structure in $\text{K}_2\text{Ru}_8\text{O}_{16}$ has a common feature with that of $\text{Ba}_{1.2}\text{Rh}_8\text{O}_{16}$ and $\text{K}_2\text{Cr}_8\text{O}_{16}$ in that the uppermost four bands in the t_{2g} manifold play a central role although the filling of electrons is different in each material.

We hope that our findings based on the electronic structure calculations on $\text{K}_2\text{Ru}_8\text{O}_{16}$ will encourage further experimental and theoretical studies of this interesting material.

ACKNOWLEDGMENTS

We would like to thank W. Kobayashi for useful comments on the experimental aspects of hollandite ruthenates and rhodates, and M. Isobe, M. Itoh, D. I. Khomskii, A. Nakao, H. Nakao, Y. Shimizu, Y. Ueda, and T. Yamauchi for useful discussions on general aspects of hollandite materials. This work was supported in part by a Grant-in-Aid for Scientific Research (No. 22540363) from the Ministry of Education, Culture, Sports, Science and Technology of Japan. A part of the computations was carried out at the Research Center for Computational Science, Okazaki Research Facilities, Japan.

¹K. Noami, Y. Muraoka, T. Wakita, M. Hirai, Y. Kato, T. Muro, Y. Tamenori, and T. Yokoya, *J. Appl. Phys.* **107**, 073910 (2010).

²M. Isobe, S. Koishi, S. Yamazaki, J. Yamaura, H. Gotou, T. Yagi, and Y. Ueda, *J. Phys. Soc. Jpn.* **78**, 114713 (2009).

³M. Isobe, S. Koishi, N. Kouno, J. Yamaura, T. Yamauchi, H. Ueda, H. Gotou, T. Yagi, and Y. Ueda, *J. Phys. Soc. Jpn.* **75**, 073801 (2006).

⁴T. Waki, H. Kato, M. Kato, and K. Yoshimura, *J. Phys. Soc. Jpn.* **73**, 275 (2004).

⁵A. Maignan, O. I. Lebedev, G. Van Tendeloo, C. Martin, and S. Hebert, *Phys. Rev. B* **82**, 035122 (2010).

⁶A. C. Komarek, Ph.D. thesis, Universitat Köln, 2009.

⁷Y. Shimizu, K. Okai, M. Itoh, M. Isobe, J. Yamaura, T. Yamauchi, and Y. Ueda, *Phys. Rev. B* **83**, 155111 (2011).

⁸Y. Ishige, T. Sudayama, Y. Wakisaka, T. Mizokawa, H. Wadati, G. A. Sawatzky, T. Z. Regier, M. Isobe, and Y. Ueda, *Phys. Rev. B* **83**, 125112 (2011).

⁹S. Horiuchi, T. Shirakawa, and Y. Ohta, *Phys. Rev. B* **77**, 155120 (2008).

¹⁰M. Sakamaki, S. Horiuchi, T. Konishi, and Y. Ohta, e-print arXiv:0811.4338.

¹¹K. Hasegawa, M. Isobe, T. Yamauchi, H. Ueda, J. I. Yamaura, H. Gotou, T. Yagi, H. Sato, and Y. Ueda, *Phys. Rev. Lett.* **103**, 146403 (2009).

¹²M. Sakamaki, T. Konishi, and Y. Ohta, *Phys. Rev. B* **80**, 024416 (2009); **82**, 099903(E) (2010).

¹³S. Ishiwata, J. W. G. Bos, Q. Huang, and R. J. Cava, *J. Phys. Condens. Matter* **18**, 3745 (2006).

- ¹⁴H. Sato, T. Enoki, J. I. Yamaura, and N. Yamamoto, *Phys. Rev. B* **59**, 12836 (1999).
- ¹⁵T. Ozawa, I. Suzuki, and H. Sato, *J. Phys. Soc. Jpn.* **75**, 014802 (2006).
- ¹⁶W. Kobayashi, *Phys. Rev. B* **79**, 155116 (2009).
- ¹⁷M. L. Foo, W. Lee, T. Siegrist, G. Lawes, A. P. Ramirez, N. P. Ong, and R. J. Cava, *Mater. Res. Bull.* **39**, 1663 (2004).
- ¹⁸Z. Q. Mao, T. He, M. M. Rosario, K. D. Nelson, D. Okuno, B. Ueland, I. G. Deac, P. Schiffer, Y. Liu, and R. J. Cava, *Phys. Rev. Lett.* **90**, 186601 (2003).
- ¹⁹A. Pautrat and W. Kobayashi, *Phys. Rev. B* **82**, 115113 (2010).
- ²⁰W. Kobayashi, S. Hebert, O. Pérez, D. Pelloquin, and A. Maignan, *Phys. Rev. B* **79**, 085207 (2009).
- ²¹T. Klimczuk, W.-L. Lee, H. W. Zandbergen, and R. J. Cava, *Mater. Res. Bull.* **39**, 1671 (2004).
- ²²J. R. Plaisier, A. A. C. van Vliet, and D. J. W. Ijdo, *J. Alloys Compd.* **314**, 56 (2001).
- ²³F. Djafri, J. Canonne, F. Abraham, and D. Thomas, *J. Less-Common Met.* **109**, 323 (1985).
- ²⁴P. Blaha, K. Schwarz, G. K. H. Madsen, D. Kvasnicka, and J. Luitz, *WIEN2k, An Augmented Plane Wave + Local Orbitals Program for Calculating Crystal Properties* (Technische Universität Wien, Austria, 2002), [<http://www.wien2k.at>].
- ²⁵V. I. Anisimov, I. V. Solovyev, M. A. Korotin, M. T. Czyzyk, and G. A. Sawatzky, *Phys. Rev. B* **48**, 16929 (1993).
- ²⁶See, e.g., T. Giamarchi, *Quantum Physics in One Dimension* (Clarendon, Oxford, 2004).
- ²⁷J. P. Perdew, K. Burke, and M. Ernzerhof, *Phys. Rev. Lett.* **77**, 3865 (1996).
- ²⁸A. I. Liechtenstein, V. I. Anisimov, and J. Zaanen, *Phys. Rev. B* **52**, R5467 (1995).
- ²⁹K. Momma and F. Izumi, *J. Appl. Crystallogr.* **41**, 653 (2008).
- ³⁰A. Kokalj, *Comput. Mater. Sci.* **28**, 155 (2003).
- ³¹D. I. Khomskii, e-print [arXiv:cond-mat/0101164](https://arxiv.org/abs/cond-mat/0101164).
- ³²C. Ambrosch-Draxl and J. O. Sofo, *Comput. Phys. Commun.* **175**, 1 (2006).